The use of an adaptive grid with TOUGH2 to track a moving phase front

Will Schreiber
Department of Mechanical Engineering
PO Box 870276
The University of Alabama Tuscaloosa, AL

ABSTRACT

Two different computer models, Computational Grid I (CGI) and Computational Grid II (CGII), are tested for their usefulness in predicting the water balance and pressure field in a porous soil surrounding a growing hemispherical melt with a surface temperature of 1700°C. The hemispherical annulus of soil is bounded on the inner radius by the melt, on the outer radius by an impervious wall, and on the planar surface by the atmosphere at 20°C and 1 atm. The motion of liquid and vapor water in the porous soil is modeled using Darcy's equation. Both computer models employ grids, which adapt to the boundary of the growing melt. CGI adapts with the melt boundary by contracting uniformly in the radial direction. In addition to adapting to the melt boundary, CGII also adapts to track the liquid-vapor interface, which moves outward from the 1700°C melt. CGII has been devised in order to attempt to reduce, at a reasonable CPU cost, numerical pressure oscillations, which arises when the grid is too coarse. A very fine CGI is used as a benchmark to test CGII and a coarser version of CGI. Results from the two CGI and the one CGII cases are presented graphically to illustrate the mass flux of liquid and vapor water and the build-up in pressure as the melt boundary approaches the impermeable wall.

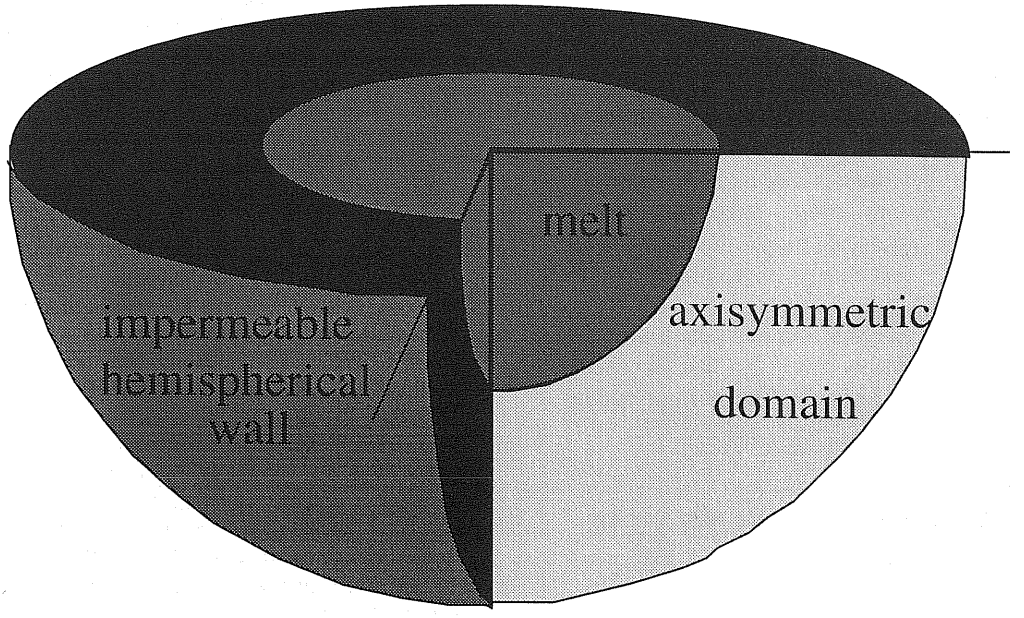

Figure 1 Illustration of the hemispherical annulus of soil bounded by the isothermal, impermeable melt interface; the impermeable outer containing wall, and the atmosphere.

INTRODUCTION

The *In Situ* Vitrification (ISV) process is currently being studied as a means for remediating soils which have been contaminated with nuclear or chemically-toxic wastes. The basic premise of the ISV process is fairly simple. Large electrodes are initially planted in the soil surrounding the contamination. Enough current is passed through the soil to raise its temperature to above melting. During the ISV process, the electrodes are continuously gravity-fed far enough into the melt to ensure that the melt reaches the depth of the contamination. After the soil containing the contaminants has been melted, it is allowed to solidify into a glass. Organic material and volatile chemical wastes are destroyed, while all other material is captured in a glass which is impervious to ground water. The necessity of handling and of transporting the wastes is virtually eliminated since they remain *in situ*. While the underlying theory behind ISV is fairly elementary, many of the details required for actually implementing the process are complicated and require thoughtful analysis for their understanding. The complications include handling the off-gas generated during the ISV process and understanding the water balance surrounding the growing melt.

The water balance in the surrounding soil is important for at least two reasons. If the object of the ISV process is to capture chemical contaminants, then one needs to know whether these contaminants, which may be carried by the water movement, will be overtaken by the melt. A second important reason for studying the water balance surrounding the melt is to be able to predict sudden pressure increases near the melt that may allow water vapor to penetrate the melt and bubble up to pressurize the off-gas containment system. The problem of sudden pressure spikes is particularly relevant in the processes when liquid water may be trapped between the growing melt front and the pit's walls.

One way to analyze the effect of a moving melt on the surrounding ground water is with computational simulation. A computer code, TOUGH2, developed by Pruess (1985, 1986) can predict the transport of heat, liquid and vapor water, air, and other species, including the effect of phase change, in a porous soil. Integral equations that describe the balance of heat and species transport relative to a control volume, V_n, are of the form,

$$\frac{d}{dt}\int_{V_n} M^{(\kappa)}\, dv = \oint (F^{(\kappa)} \cdot \hat{n}) + \int_{V_n} q^{(\kappa)}\, dv \qquad (1)$$

where: $\kappa = 1$: water, $\kappa = 2$: air, and $\kappa = 3$: heat.

The finite difference formulation and solution of equation (1) as well as the equations that define $M^{(\kappa)}$, the accumulation of mass (or heat), $F^{(\kappa)}$, the transfer of mass or heat, $q^{(\kappa)}$, the source of mass or heat, and constitutive equations are described by Pruess (1985, 1986).

Equation (1) may be expressed as in implicit finite difference in time in terms of a residual, which is set equal to zero,

$$R_n^{(\kappa)k+1} = M_n^{(\kappa)k+1} - M_n^{(\kappa)k} - \frac{\Delta t}{V_n}\left(\sum_m A_{nm} F_{nm}^{(\kappa)k+1} + V_n q_n^{(\kappa)k+1}\right) = 0. \qquad (2)$$

The Newton-Raphson method is used to update all unknown variables implicitly in equation (2) as well as the ancillary equations.

For the present project, two modified versions of the TOUGH2 code are considered and tested on a problem whose geometry is illustrated in figure 1. The parameters for the test case are given in table 1. The first version of TOUGH2 has been modified to solve the transport equations on a relatively fine grid (CGI) which is uniform in the radial direction and adapts uniformly to the growing melt boundary. (See figure 2.) The second version of TOUGH2 uses a doubly adaptive grid (CGII) which moves with both the external boundary (the melt front) and internal boundary (the liquid/vapor phase front). (See figure 3.) As the melt front progresses, CGII is continuously reconfigured to fit the changing external and internal boundaries. A thin line of small cells captures the liquid/vapor phase front and "ferry" it across the domain that represents the drying soil.

Kuo and Schreiber (1994), Haywood et al (1994), Lee and Yeh (1994), Gottardi and Venutelli (1994), and Zhang and Moallemi (1995) have recently published articles describing the use of adaptive grids with transport problems. Thompson (1985) describes many of the general considerations for this type of problem.

NUMERICAL METHOD

Both CGI and CGII have in common the ability to adapt to an inner spherical boundary whose radius increases with time. Both grids are constructed from lines (spokes) which increase in the radial direction along fixed angular coordinates and lines which increase in the angular direction. The two sets of grid lines intersect at nodes, which can slide along the spokes to fit the changing inner boundary. The melt front moves continuously throughout the computation and the grid has to be regenerated at every time step to keep pace with the changing boundary. The amount that the spokes' lengths shorten with every time step is determined as the product of the melt front velocity and the length of the time step.

The grid is updated and the lengths between cells, the interface areas, and the cell volumes are recalculated to suit the new grid location. New node locations are determined as a simple interpolation along the spokes since only one boundary, the melt interface, changes location. In order to maintain constant relative radial distances between the nodes, the distances between nodes are divided by the ratio of the total spoke length before and after the melt movement.

The original TOUGH2 code has an adaptable time step length. If the Newton-Raphson iteration cannot converge for a given time step, that time step is decreased prior to another attempt at convergence. To accommodate the adaptive time step, the grid values prior to the time step are saved in order to recalculate the new grid in the event that a reduced time step is necessary for convergence.

Melt radius Initial: 1.0 m; Final: 1.9 m Melt Boundary: Isothermal @ 1700°C; impermeable Hemispherical growth: 4.4 x 10^{-5} m^3/s Outer Boundary: Solid impermeable wall; radius: 2.0 m mass: 15,250 kg; specific heat: 700 J/kg·K initial temperature 20°C Upper Boundary: Permeable; Atmospheric pressure; 20°C	Soil: Density: 2600 kg/m^3: Sp. heat of grain: 700 J/kg·K Initial Temp.: 20°C; Initial liquid sat. 0.2; Porosity: 0.4 Conductivity (fully saturated) 1.13 W/m K; Permeability: 10^{-12} m2; Saturation of immobile water: 0.15 Reference pressure: 632 kPa Capillary Pressure Model: Leverett's (1941) function Relative Permeability: Fatt and Klikoff (1959)

Table 1 Parameters and boundary conditions for test problem.

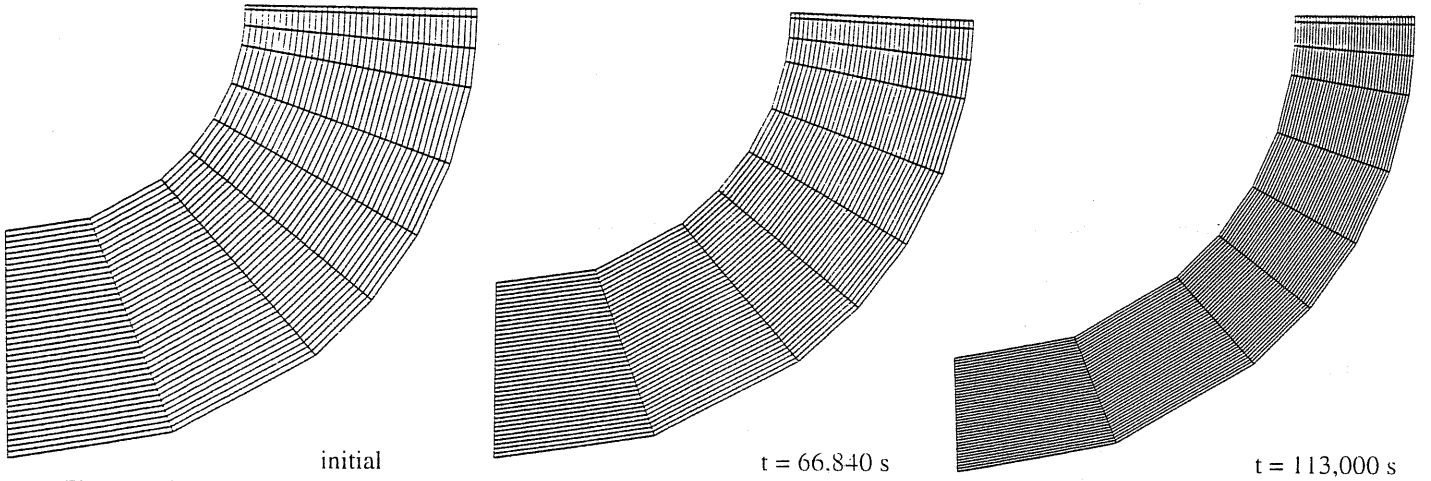

Figure 2 CGI contracts radially to adapt to the increasing radius of the melt interface.

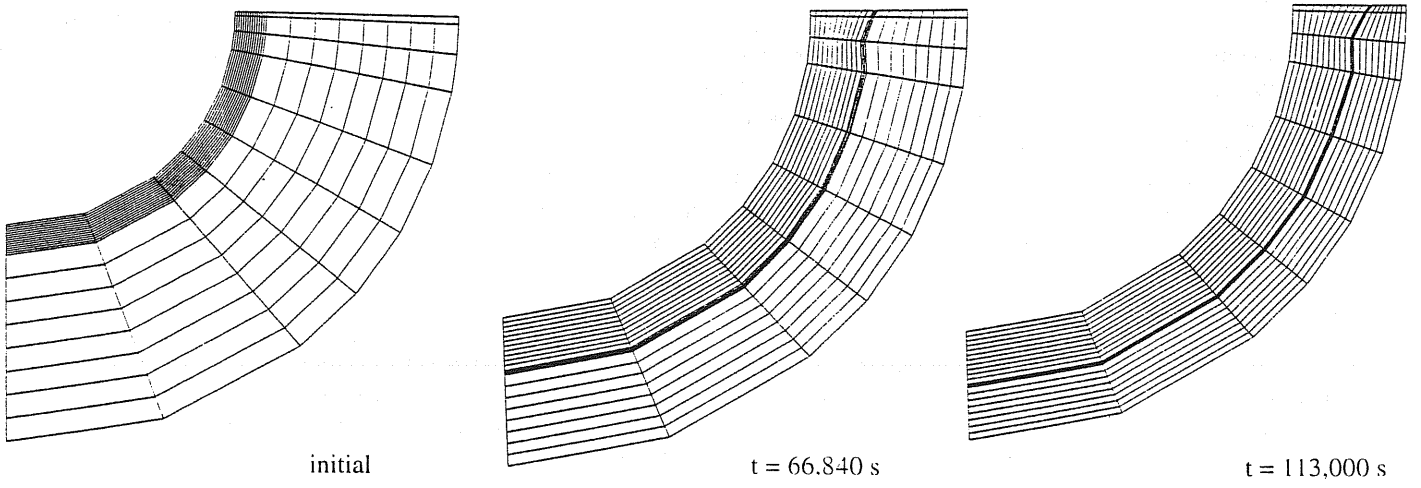

Figure 3 CGII adapts to the increasing radius of the inner boundary and to the moving vapor-liquid interface. Three narrow cells move with and contain the vapor-liquid interface.

Thompson (1985) has demonstrated that the cell interface moving with an adaptive grid effectively experiences an advective flow due to the Lagrangian grid movement. The advective flow due to the Lagrangian grid movement is added to the advection due to fluid motion relative to the Eulerian grid. For the static grid, the flux of heat or mass is a combination of diffusive and advective transport modes. In the case of flow in a porous media, the conduction mode is mainly confined to heat conducted in the rock matrix. The advection transport consists of fluid motion through the matrix. Including the effect of a moving grid as an advective term causes the flux for conduction in the radial direction, to be modified as,

$$q_{conduction} = \left[-K_{nm} \frac{T_m - T_n}{r_m - r_n} - \rho\, c_p\, v_{grid} \left(1-\Phi\right) T_m \right] A_{nm} \tag{3}$$

The time-dependency of a cell's volume must also be included in the solution procedure to correctly account for mass and enthalpy conservation. The Newton-Raphson solution technique is used for solving the nonlinear equations. To account for the cell volume change over the course of the time step, the variable at the old time value is multiplied by the ratio of the old cell volume by the new cell volume. This variation of volume with time accounts for the effect of grid movement on the mass advection.

The grid CGII has been devised in an effort to eliminate the pressure oscillation problem associated with the boiling and subsequent dry-out of the cells. In addition to adapting like CGI, CGII can also adapt to track the interface between the saturation region and the vapor region. Using an adaptive grid, the interface can be held within three special narrow cells which move prior to drying out and ferry the interface across the domain. In the initial grid, the seven cell layers closest to the hub are very fine. Fifteen large cell layers extend between the finely packed layer of cells and the outer boundary. As the grid adapts to the changing solution, the grid nodes are allowed to move along the rigid spokes. Since the nodes along a given spoke move independently of the nodes of the other spokes, the grid is flexible enough to adapt to a time-dependent vapor phase front whose radial growth rate varies with angle.

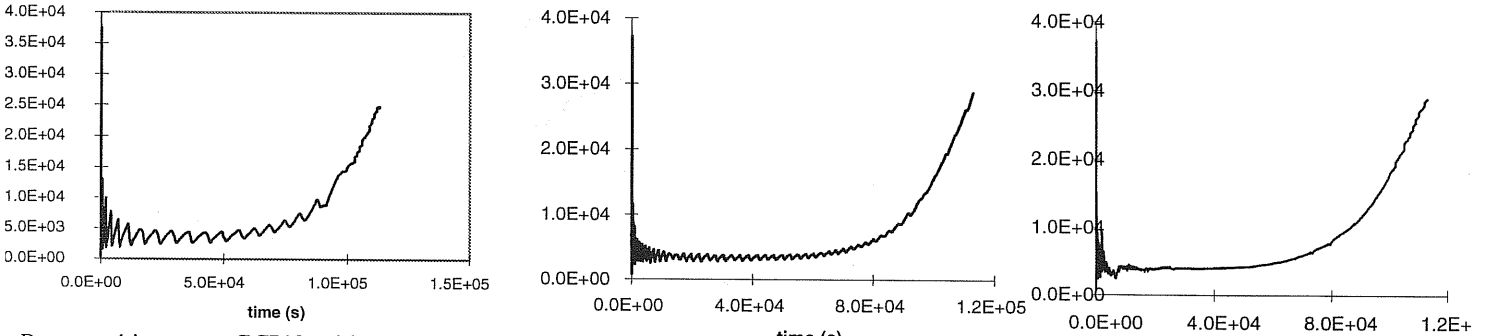

Pressure history on GCI40 grid

Pressure history using CGI100

Pressure history using CGII

Figure 4 . Pressure history on melt surface at $\phi = \pi$. Illustration on the left shows pressure oscillation problem experienced when CGI is too coarse. Two illustrations on the right compare pressure histories as predicted by CGI with 100 uniform cell divisions in the radial direction and CGII with 22 cell divisions with adapting lengths in the radial direction.

For the grid's adaptation to the movement of the vapor phase front, several issues had to be considered. A means had to be devised for maintaining the vapor front within two narrow cells while the cells in the direction toward the inner hub had to expand and the cells toward the outer rim had to compress as the special cell moved. With each time step, a decision is made whether a node should move along its spoke and, if so, how far the cell's nodes should move to capture the vapor interface within the narrow cell. To effect the cell moves, the value of vapor saturation at the nodes is determined as well as moving the grid without disturbing the spatial distribution of thermodynamic properties within the problem domain. In order not to interfere with the calculation of the grid generation due to melt front movement, a special short time step is used whenever the grid is required to adapt to the vapor-liquid front. During this shortened time step, the melt movement is turned off and the primary properties are allowed to come to equilibrium (through numerical iterations within the time step). After the special time step, the length of the time step is subtracted from the sum total time of the computation. It was found that moving the cells at every angular value all at once is better than allowing the different sets of constant angle cells to move higgledy-piggledy. Whenever the criteria for moving is met for any group of special cells, the required movement is determined for every set of constant-angle special cells. The one-for-all, all-for-one cell movement approach ensures better convergence and fewer disruptions in the program's time stepping.

When the thickness of the cell layers located between the special cells and the outer rim are less than a specified minimum value, the grid ceases to adapt to follow the vapor phase front and the outer cells are allowed to dry out.

RESULTS

As discussed in the "numerical methods" section above, figure 1 illustrates the problem geometry. Table 1 lists the parameters and boundary conditions of the problem. The saturated water in the soil is vaporized as heat is transferred

from the melt interface to raise the temperature of the surrounding soil above the boiling point. The pressure surrounding the melt rises due to the creation of vapor at a rate which is larger than the rate the vapor escapes from the soil into the atmosphere as well as due to the decreasing volume of the soil region in which the vapor is confined.

Two CGI grids and one CGII grid are compared for their ability to simulate the water-vapor balance and pressure distribution for the problem described above. A CGI grid with 100 radial cell divisions (CGI100) was used as a benchmark by which to compare a coarser CGI grid, with 40 radial cell divisions (CGI40), and an adaptive CGII with 22 radial cell divisions. CGI40 was the coarsest grid used that allowed convergence of the solution to 295,000s. For all three grid configurations, the angular direction was divided into 9 divisions as illustrated in figures 2 and 3.

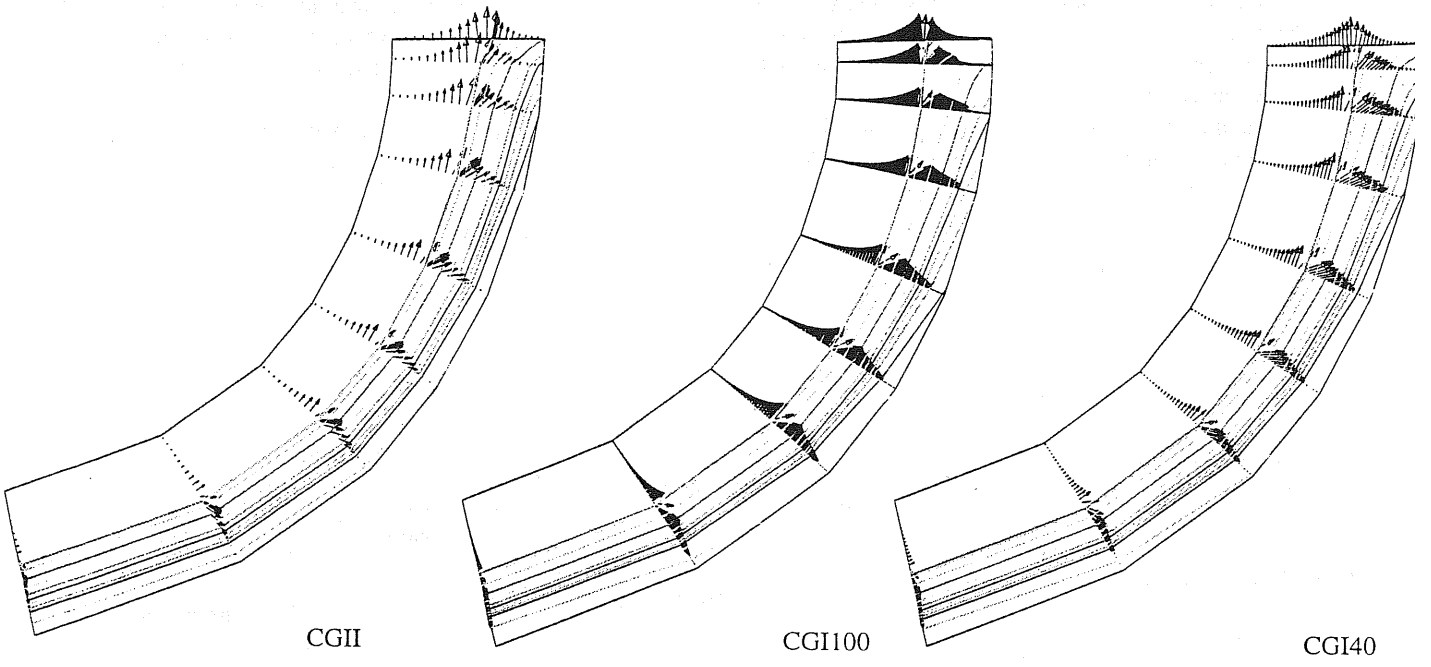

Figure 5 Comparison of vapor mass flux, $\dot{m}_g$, and liquid saturation, s_l, distribution at 113,000s when melt radius is at 1.5 m. Maximum $\dot{m}_g$ (kg/m^2·s) / s_l: CGII: 1.05x10^{-3} / 0.80, CGI40: 7.77x10^{-4} / 0.87, CGI100: 9.02x10^{-4} / 0.78

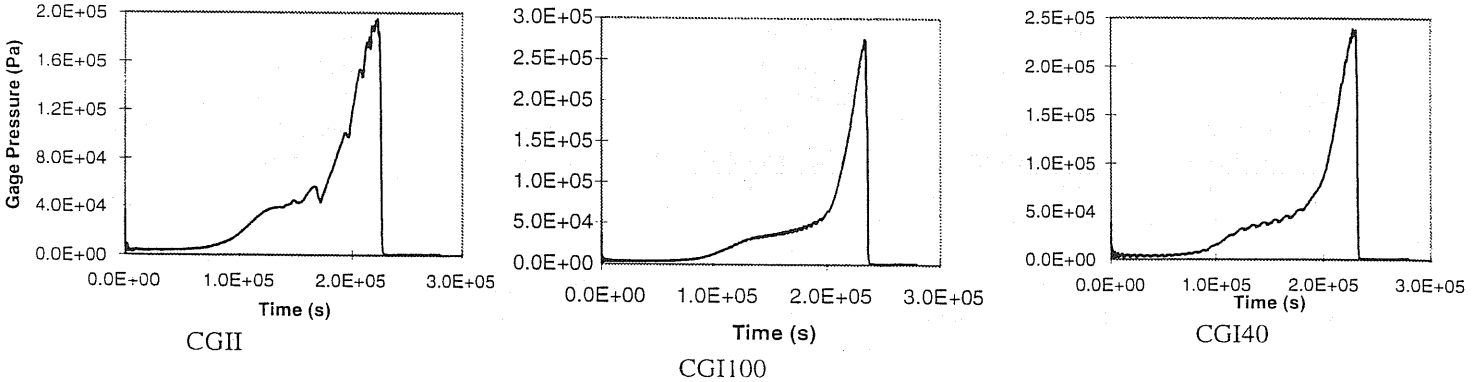

Figure 6 Comparison of pressure histories to 295,000s when melt radius reaches 1.90 m. CPU times on the IBM RS6000 model 520: CGII - 86,500 s; CGI100 - 660,700 s; CGI40 - 88,600 s.

In figure 4, it is seen that the use of CGII is effective for virtually eliminating the pressure oscillations. Even with 100 radial cell divisions, CGI still exhibits noticeable pressure oscillations over the time period of 113,000 s. In figure 5, the mass flux of vapor and the liquid saturation is depicted. The soil is dried out (containing only water vapor) to a radial location approximately halfway between the melt and outer wall. The mass of vapor being transported toward the soil surface in the dried out region is approximately the same as that in the wet region. The vapor mass flux just outboard of

the dry out region exhibits a strong component of radial velocity because of the vapor generation at this interface. Some of the outward flow of vapor recondenses when it reaches the cooler soil to cause the highest liquid saturation to exist near the outer wall. At 41,000 s, this recondensed vapor forms a layer between two drier regions of soil. By 113,000 s, this layer has reached the outer wall.

As the average liquid saturation in the soil between the melt and the outer wall increases, a higher rate of boiling occurs at the vapor-liquid interface. The increased generation rate of vapor combined with the narrowing of the soil channel between the melt and the outer wall cause the pressure level at the lowest point of the melt's surface to rise. Figure 6 illustrates the gage pressure history of the point at the line of symmetry on the melt's surface. At about 200,000 s, the pressure is seen to spike. The maximum gage pressure peak is predicted by CGI100 to reach 2.74 bar at 234,000 s, by CGI40 to reach 2.39 bar at 228,000 s, and by CGII to reach 1.95 bar at 223,000 s. CGI40 and CGII require about the same amount of CPU on the IBM RS6000 model 320 workstation. CGI40's spurious pressure oscillation illustrated in figure 4 does not seem to have adversely affected the prediction of the pressure history. The radial grid separation decreases as the simulation progresses; consequently, pressure oscillation diminishes. On the other hand, CGII's overprediction of liquid water loss through the soil's surface and the subsequent decreased fraction of water that remains before the pressure spike causes a pressure spike of somewhat lower magnitude than CGI100.

CONCLUSIONS

1. Computational prediction of the water-vapor transport around an ISV melt growing in soil confined by an impermeable wall can be useful for predicting pressure spikes.
2. The CGI model needs to be verified using experimental or analytical data for comparison but seems to offer a viable means to model heat and mass transport in the soil around an ISV melt.
3. The CGII does not currently offer any advantage over the CGI.
4. The CGII may be useful for modeling other ISV water balance problems in which a computational grid does not contract with the progression of time.

REFERENCES

Fatt, I. and Klikoff, W. A., 1959, "Effect of Fractional Wettability on Multiphase Flow through Porous Media" AIME Transactions, vol. 216, p. 246.

Fredlund, D. G. and Rahardjo, H., 1993, *Soil Mechanics for Unsaturated Soils*, Wiley-Interscience Publication.

Gottardi, G. and Venutelli, M., 1994, "One-Dimensional Moving Finite-Element Model of solute Transport", *Ground Water*, vol. 32, pp. 645 - 649.

Haywood, R. J., Renkisbulut, M., and Raithby, G. D., 1994, "Numerical Solution of Deforming Droplets at Intermediate Reynolds Numbers", *Numerical Heat Transfer, Part A*, vol. 26, pp. 253 - 272.

Kuo, C. H. and Schreiber, W. C., 1994, "An Interface Tracking Method for Solving Pure Substance Phase change Problems Using Nonsteady Curvilinear Coordinates", *Current Developments in Numerical Simulation of flow and Heat Transfer* (HTD-Vol. 275), pp. 57 - 64, ed. K. Vafai and J. L. S. Chen.

Lee, D. and Yeh, C. L., 1994, "Computation of Turbulent Recirculating Flows Using a Hybrid Adaptive Grid", ", *Numerical Heat Transfer, Part A*, vol. 26, pp. 415 - 430.

Leverett, M. C., 1941, "Capillary Behavior in Porous solids, AIME Trans., vol. 142, p. 152.

Pruess, K. and Narasimhan, T. N., 1985, "A practical Method for Modeling Fluid and Heat Flow in Fractured Porous Media", Society of Petroleum Engineers Journal, vol. 25, pp 14 - 26.

Pruess, K., 1986, *TOUGH User's Guide*, Sandia National Laboratories research report (NUREG/CR-4645, SAND 86-7104, RW)

Thompson, J. F., Warsi, Z. U. A., and Mastin, C. W., 1985, *Numerical Grid Generation: Foundations and Applications*, North-Holland, New York.

Udell, K. S. and Fitch, J. S., 1985, Heat and Mass Transfer in Capillary Porous Media Considering Evaporation, condensation, and Non-Condensible Gas Effects, 23rd ASME/AIChE National Heat Transfer Conference, Denver, Co..

Zhang, Hui and Moallemi, M. K., 1995, "Numerical Simulation of Hot-Dip Metallic Coating Process", *Int. J. Heat Mass Transfer*, vol. 38, pp. 241 - 257.